

# Reachability Analysis of Power System Frequency Dynamics with New High-Capacity HVAC and HVDC Transmission Lines

Hugo N. Villegas Pico, Dionysios C. Aliprantis  
 Department of Electrical and Computer Engineering  
 Iowa State University  
 Ames, IA 50011 USA  
 Email: {hvvillega, dali}@iastate.edu

Elena C. Hoff  
 Department of Physics  
 Lewis and Clark College  
 Portland, OR 97219 USA  
 Email: ehoff@lclark.edu

## Abstract

This paper presents a computational technique for conducting assessments of multi-area power system frequency dynamics using reachability analysis theory. To this end, a reduced-order model of the U.S. power system with high renewable penetration is derived. We investigate the control capabilities of HVDC lines to improve the frequency response of asynchronously connected regions, and to transmit the variability of renewable sources within synchronously connected areas. In this modeling framework, disturbances and parameters are treated as belonging to unknown-but-bounded sets. The analysis yields bounds that are guaranteed to contain the trajectories of all possible scenarios.

## Introduction

The rapid integration of renewable energy sources into the electric grid has made the transmission expansion within the continental U.S. a topic of interest. In particular, the fact that wind resources are located in geographically remote areas relative to the large load centers has motivated research on the design of a transmission overlay at the national level [1], which could yield significant environmental and economical benefits [2].

An important metric of power system operation is frequency. Recent work has investigated the impacts on system inertia due to high penetration of wind energy [3]–[6]. In these studies, the frequency response of the three U.S. interconnections has been evaluated under various scenarios, where a mix of conventional thermal generation and wind power plants supply the system load. The results are obtained with the existing transmission system, but it is recognized that investments in transmission infrastructure are necessary [6].

In this paper, we propose a computational technique that can be used to assess, at a planning stage, the power system frequency dynamics when new high-capacity HVAC and HVDC transmission lines are built. In particular, the controls of HVDC lines include frequency feedback loops [7]–[11]. This permits the distribution of the negative impacts of a sudden generation-load unbalance among asynchronously connected areas, but it also helps transfer disturbances within syn-

chronously connected areas, when HVDC lines are embedded within an interconnection.

The proposed algorithm is based on reachability analysis of dynamic systems [12]–[14]. This framework is attractive because it can capture several kinds of uncertainties, such as parametric and input/disturbance uncertainties. Here, uncertainties are modeled as belonging to unknown-but-bounded sets, in contrast to probabilistic approaches [15]–[17]. The advantage of this modeling approach is that one does not need to provide information about the required probability distributions. The method calculates the evolution of reachable sets over time, which are guaranteed to contain the state trajectories under all possible scenarios.

The paper is structured as follows. First, a brief introduction to reachability theory and a concise description of the underlying computational method is given. Next, we describe the general power system modeling framework. Then, implementation case studies are provided, and conclusions are drawn.

## Zonotope-Based Reachability Analysis of Linear Systems

In systems theory, reachability analysis addresses the computation of sets (also called flow pipes) that contain all possible trajectories of an uncertain dynamic system [13], [14]. In this paper, we model the power system as an uncertain linear time-invariant system with given sets of unknown-but-bounded parameters, inputs, disturbances, and initial conditions, which can be represented by<sup>1</sup>

$$\frac{dx(t)}{dt} = Ax(t) + v(t), \text{ with } A \in \mathcal{A} \subset \mathbb{R}^{n_x \times n_x}, \\ v(t) \in \mathcal{V} \subset \mathbb{R}^{n_x}, x(t_0) \in \mathcal{X}_0 \subset \mathbb{R}^{n_x} \quad (1)$$

where  $A$  is an uncertain constant matrix belonging to a set  $\mathcal{A}$ ,  $v(t)$  is an uncertain generalized input/disturbance vector in a set  $\mathcal{V}$ , and  $x(t_0)$  is an uncertain initial condition in a set  $\mathcal{X}_0$ . Sets are assumed to be convex. The solution of (1) is a time-varying set, called the reachable set, that contains all possible trajectories of the states through time.

<sup>1</sup>This is a compact form of  $dx(t)/dt = Ax(t) + Bu(t) + Ww(t)$  with  $v(t) = Bu(t) + Ww(t)$ , where  $u$  and  $w$  are inputs and disturbances, respectively.

The exact reachable set  $\mathcal{R}^e(t)$  of a dynamic system (1) at time  $t$ , starting from time  $t_0$ , is

$$\begin{aligned}\mathcal{R}^e(t) &\triangleq \{x(t) : x(t) \text{ is a solution of (1), } \forall A \in \mathcal{A}, \\ &\quad \forall v(\tau) \in \mathcal{V}, \forall x(t_0) \in \mathcal{X}_0, \text{ and } \tau \in [t_0, t]\}.\end{aligned}\quad (2)$$

An over-approximation  $\mathcal{R}(t)$  of the exact reachable set is one that satisfies  $\mathcal{R}^e(t) \subseteq \mathcal{R}(t)$ . In general, the calculation of  $\mathcal{R}(t)$  is more tractable than finding  $\mathcal{R}^e(t)$ . However, one should seek sets that enclose  $\mathcal{R}^e(t)$  as tightly as possible. An over-approximation of a reachable set over a time interval  $[t_0, t]$  is defined by taking the union of reachable sets computed at discrete (appropriately spaced) time points  $t_k \in [t_0, t]$ ,  $k = 1, \dots, K$ :

$$\mathcal{R}([t_0, t]) = \bigcup_k \mathcal{R}([t_{k-1}, t_k]).\quad (3)$$

Various methods have been proposed for the computation of over-approximations of reachable sets of linear systems, using, e.g., ellipsoids [18]–[20], polytopes [13], [14], and zonotopes [21], [22]. Notably, the theory has found only a limited number of applications (so far) in power engineering [14], [20].

The computational method adopted herein is the one proposed for linear systems in [21], [22] based on representing reachable sets by zonotopes. A zonotope  $\mathcal{Z}$  is a set defined by

$$\mathcal{Z} = \left\{ x = c + \sum_{i=1}^p \alpha_i g^{(i)}, -1 \leq \alpha_i \leq 1 \right\}\quad (4)$$

where  $x$ ,  $c$ , and  $g^{(i)}$  are vectors of  $\mathbb{R}^n$ . A shorthand notation for a zonotope is:  $\mathcal{Z} = (c, \langle g^{(1)}, \dots, g^{(p)} \rangle)$ . The vectors  $g^{(1)}, \dots, g^{(p)}$  are called the generators of the zonotope  $\mathcal{Z}$ , and  $c$  is its center.

This numerical technique also uses results from interval analysis. An interval number  $\beta$  is a numerical set  $\beta = [\underline{\beta}, \bar{\beta}]$  bounded by two real numbers  $\underline{\beta}$  and  $\bar{\beta}$  with  $\underline{\beta} \leq \bar{\beta}$ . This definition can be extended to interval vectors and matrices. An interval vector (or simply a ‘box’) of dimension  $n$  is a pair  $\underline{x} = [\underline{x}, \bar{x}]$  consisting of two real column vectors  $\underline{x}$  and  $\bar{x}$  of length  $n$  with  $\underline{x}_i \leq \bar{x}_i$  ( $i = 1, 2, 3, \dots, n$ ). Similarly, an interval matrix is an  $n \times n$  matrix  $\underline{M}$  whose entries  $M_{ij} = [\underline{M}_{ij}, \bar{M}_{ij}]$  ( $i, j = 1, 2, 3, \dots, n$ ) are intervals.<sup>2</sup>

An advantage of using zonotopes is computational efficiency for systems with relatively high dimensions. This is due to the simplicity of set representations using zonotopes, together with the fact that they are closed under linear transformations and Minkowski sums. Hence, operations can be efficiently processed on a computer, in contrast with other set representations such as polytopes or ellipsoids [24, Ch. 2, p. 32]. Please refer to the Appendix for further details.

A summary of the main steps involved in the computation of reachable sets for linear systems as in (1) are provided below.

<sup>2</sup>Standard notation and definitions for interval analysis are adopted from [23]. Lowercase boldface letters are used for interval (column) vectors, whereas uppercase boldface letters are used for interval matrices.

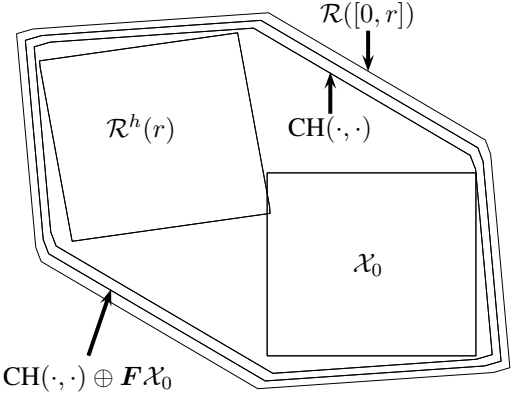


Fig. 1. Depiction of basic steps involved in the computation of the reachable set [21], [22].

### Step 1: Computation of $\mathcal{R}(r)$

First, we find an expression of the reachable set  $\mathcal{R}(r)$  (starting at  $t_0 = 0$  and progressing for a “short” time step  $r > 0$ ) under the influence of an input  $v(\cdot) \in \mathcal{V}$  and initial condition  $\mathcal{X}_0$ . To this end, an over-approximation of the exact reachable set (2) at  $t = r$  is formulated as follows [22]

$$\mathcal{R}^e(r) \subseteq \mathcal{R}(r) = \underbrace{[\mathbf{e}^{\mathbf{A}r}] \mathcal{X}_0}_{\mathcal{R}^h(r)} \oplus \underbrace{\int_0^r \mathbf{e}^{\mathbf{A}\tau} d\tau \mathcal{V}}_{\mathcal{R}^f([0, r])}.\quad (5)$$

Here,  $\mathbf{A} \supseteq \mathcal{A}$  is an interval matrix that captures the parameter uncertainty, and  $\mathcal{X}_0$  and  $\mathcal{V}$  are zonotopes. The first  $[\cdot]$  operator returns an interval matrix that over-approximates  $e^{\mathbf{A}r}$  for all  $A \in \mathcal{A}$ ; the second  $[\cdot]$  operator returns a zonotope that over-approximates the integral [22], [25]. Two zonotopes can be defined, viz., a homogeneous solution zonotope  $\mathcal{R}^h(r)$  and a forced solution zonotope  $\mathcal{R}^f([0, r])$ . These are used for the computation of  $\mathcal{R}([0, r])$  in the next step.

### Step 2: Computation of $\mathcal{R}([0, r])$

The reachable set  $\mathcal{R}([0, r])$  is found by computing a convex hull zonotope that encloses (as tight as possible)  $\mathcal{X}_0$  and  $\mathcal{R}^h(r)$ , denoted by  $\text{CH}(\mathcal{X}_0, \mathcal{R}^h(r))$  [21]. Then, this set is bloated (via Minkowski addition) with a zonotope  $\mathbf{F} \mathcal{X}_0$  to account for the curvature of all trajectories within the time interval  $[0, r]$  [22]. Finally, the resulting set and the forced reachable set  $\mathcal{R}^f([0, r])$  are Minkowski-added to obtain  $\mathcal{R}([0, r])$ . These operations are depicted in Fig. 1, and can be expressed as

$$\mathcal{R}([0, r]) = (\text{CH}(\mathcal{X}_0, \mathcal{R}^h(r)) \oplus \mathbf{F} \mathcal{X}_0) \oplus \mathcal{R}^f([0, r]).\quad (6)$$

### Step 3: Computation of $\mathcal{R}([0, t])$

For the computation of  $\mathcal{R}([0, t])$ , zonotope sets of the form

$$\mathcal{R}([kr, (k+1)r]) = \left( [\mathbf{e}^{\mathbf{A}r}] \mathcal{R}([(k-1)r, kr]) \right) \oplus \mathcal{R}^f([0, r])\quad (7)$$

are computed iteratively from  $k = 1$  to  $k = K = \text{ceil}(t/r)$ . An over-approximation of the reachable set for the dynamic system (1) is obtained by (3).

#### Step 4: Computation of Time-Domain Bounds $\mathbf{x}(\tau)$

Time-domain bounds of system states are obtained by finding the interval hulls of each computed zonotope  $\mathcal{R}([(k-1)r, kr])$  as follows

$$\mathbf{x}([(k-1)r, kr]) = \text{IH}(\mathcal{R}([(k-1)r, kr])) \quad (8)$$

for  $k = 1, \dots, K$ , where

$$\text{IH}(\mathcal{Z}) = [c - w, c + w] \text{ with } w = \sum_{i=1}^p |g^{(i)}|. \quad (9)$$

This is an optional step, which is useful for plotting bounds of individual states as functions of time.

## Power System Modeling

The adopted power system modeling approach is conceptualized in Fig. 2 using a generic 4-area system, where each area contains one equivalent synchronous generator. In this simple example, area  $a$  is a high-inertia area, connected synchronously to areas  $b$  and  $c$ , which have lower inertia, and there is substantial renewable penetration in area  $b$ . An HVDC line embedded within this interconnection transmits renewable power and its variability  $p^{lr}$  (i.e., oscillatory components below a certain frequency) from the low-inertia area  $b$  to the high-inertia area  $a$ . Area  $d$  is a lower-inertia area compared to area  $a$ , and has high penetration of renewables. It is asynchronously tied to the  $abc$  interconnection through a frequency-sensitive HVDC line, which injects a power component  $p^{l\omega}$  on top of its normal dc transmission level, to improve its frequency response.

This modeling approach is based on the following assumptions [26]–[29]:

- All generators within an area are tightly connected with negligible synchronizing oscillations.
- All generators within an area can absorb any load change proportionally to their capacity without any network constraints.
- The dynamics of conventional generation within an area are thermally dominated and, for simplicity, are represented by single steam chest time constants (i.e., steam reheating is not modeled).
- Renewable generation and demand within an area do not contribute to the inertial response, hence they are modeled as power injections.
- The inter-area HVAC and HVDC transmission system is lossless.
- There are no communication delays from remote measurements.
- The system dynamics are linear around an equilibrium point, and all dynamic variables are expressed as p.u. deviations from this point.

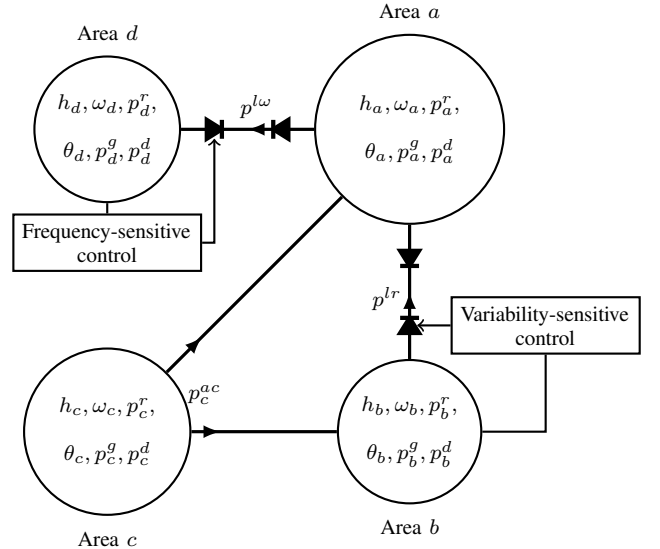


Fig. 2. Multi-area power system setup with synchronous and asynchronous interconnections (HVAC and HVDC transmission).

The equivalent rotor frequency dynamics of an area  $i$ , in a general  $n$ -area bulk power system, can be written as

$$\frac{d\omega_i}{dt} = \frac{1}{2h_i} (p_i^g + p_i^r - p_i^d - p_i^{ac} + p_i^{dc\omega} + p_i^{dc\sigma}) \quad (10)$$

where  $\omega_i(t)$  is the equivalent rotor frequency of area  $i$ ,  $h_i$  is the equivalent rotor inertia constant of area  $i$ ,  $p_i^g(t)$  is the conventionally generated power in area  $i$ ,  $p_i^r(t)$  is the renewable power generated in area  $i$ ,  $p_i^d(t)$  is the power demand in area  $i$ ,  $p_i^{ac}(t)$  is the total power withdrawn by the HVAC tie lines connected to area  $i$ ,  $p_i^{dc\omega}(t)$  is the total injected power by the HVDC frequency-sensitive lines connected to area  $i$ , and  $p_i^{dc\sigma}(t)$  is the total injected power by the HVDC variability-sensitive lines connected to area  $i$ . Therefore, the frequency dynamics of all areas can be expressed in matrix-vector form as

$$\frac{d\omega}{dt} = \frac{1}{2} H^{-1} (p^g + p^r - p^d - p^{ac} + p^{dc\omega} + p^{dc\sigma}) \quad (11)$$

with  $H = \text{diag}(h_1, \dots, h_n)$ .

The aggregated dynamics of conventional generators (non-reheat turbines) are approximated with a first-order dynamic system [27], [29]

$$\frac{dp^g}{dt} = -T_g^{-1} (p^g - K_g u^{cg}) \quad (12)$$

where  $T_g = \text{diag}(\tau_{g1}, \dots, \tau_{gn})$  is a matrix of time constants of the aggregated generators,  $K_g = \text{diag}(k_{g1}, \dots, k_{gn})$  is a matrix of gain parameters, and  $u^{cg}$  is a governor command vector.

The governors are modeled as proportional-integral compensators as depicted in Fig. 3 [27], [29]. Hence,

$$u^{cg} = v^{cg} - K_c (\omega + R_c p^g) \quad (13)$$

and

$$\frac{dv^{cg}}{dt} = -T_c^{-1} K_c (\omega + R_c p^g) \quad (14)$$

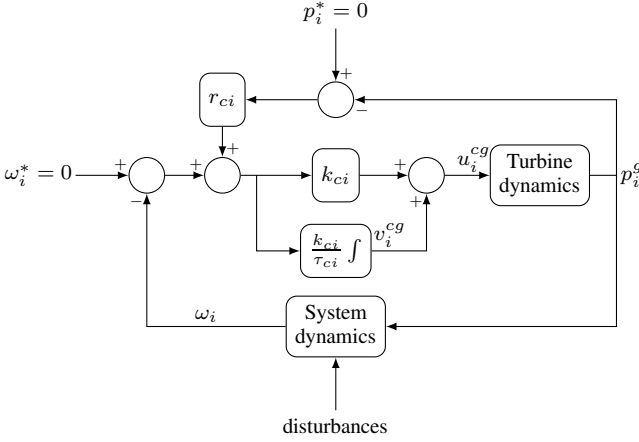


Fig. 3. Governor control block diagram.

where  $T_c = \text{diag}(\tau_{c1}, \dots, \tau_{cn})$ ,  $K_c = \text{diag}(k_{c1}, \dots, k_{cn})$ , and  $R_c = \text{diag}(r_{c1}, \dots, r_{cn})$  are matrices with integrator, proportional, and power droop constants, respectively.

The variability due to renewable energy sources is modeled by an unknown-but-bounded time-varying disturbance vector  $p^r(t) \in \mathcal{W}^r$ . The variability of demand is modeled as

$$p^d = w^d + D\omega \quad (15)$$

using unknown-but-bounded terms  $w^d(t) \in \mathcal{W}^d$ , and damping  $D = \text{diag}(d_1, \dots, d_n)$ ,  $d_i \geq 0$  [27].

Inside a synchronously connected region  $R$ , the powers withdrawn from  $R$  by HVAC lines are expressed as

$$p_R^{ac} = B'_R \theta_{\Delta R} \quad (16)$$

where  $B'_R$  is a reduced network susceptance matrix, obtained by referring all rotor angles to a given area  $k$  in region  $R$ .

This formula can be expanded to represent a bulk power system with several interconnections. For example, for a three-interconnection power system like the U.S., the power withdrawn from every area can be expressed as

$$p^{ac} = B' \theta_{\Delta} \quad (17)$$

with

$$B' = \begin{bmatrix} B'_{R1} & 0 & 0 \\ 0 & B'_{R2} & 0 \\ 0 & 0 & B'_{R3} \end{bmatrix} \text{ and } \theta_{\Delta} = \begin{bmatrix} \theta_{\Delta R1} \\ \theta_{\Delta R2} \\ \theta_{\Delta R3} \end{bmatrix} \quad (18)$$

where  $\theta_{\Delta R1}$ ,  $\theta_{\Delta R2}$ ,  $\theta_{\Delta R3}$ , are vectors of referred rotor angles, each one with respect to a given area angle within its own interconnection.

The integration of a new HVAC transmission overlay by building new lines connecting the nodes of an existing transmission system can be represented by modifying the reduced susceptance matrix as

$$B' = B^{e'} + B^{o'} \quad (19)$$

that is, as the sum of an existing  $B^{e'}$  and an overlay  $B^{o'}$  reduced susceptance matrix.

The dynamics of the referred angles in (16) can be written as

$$\frac{d\theta_{\Delta}}{dt} = \omega_e I' \omega \quad (20)$$

with  $\omega_e = 120\pi$  rad/s and  $I'$  a matrix mapping that refers each area's frequency to the reference speed of area  $k$  within an interconnection, i.e.,  $d\theta_{\Delta i}/dt = \omega_e(\omega_i - \omega_k)$ , for  $i = 1, \dots, n$ ,  $i \neq k$ . For a multi-interconnection power system,  $I'$  is modified similarly to the susceptance matrix in (18).

HVDC lines between two asynchronous interconnections can be equipped with frequency-sensitive controls. This capability can reduce the impact of a low-frequency event in an interconnection with relatively low inertia by injecting power drawn from the other interconnection that has high inertia and power capacity. (More precisely, this is achieved by modulating the constant component of power flowing when the disturbance occurs.) To capture this, the power transmitted by a number  $s_1$  of frequency-sensitive HVDC lines  $p^{l\omega}$  is mapped into areal power injections  $p^{dc\omega}$  by

$$p^{dc\omega} = M^{\omega} p^{l\omega} \quad (21)$$

where the entries of the  $n \times s_1$  matrix  $M^{\omega}$  belong to  $\{-1, 0, 1\}$  (each column has exactly one pair of  $+1$  and  $-1$  terms). The frequency-sensitive components of the transferred power  $p^{l\omega}$  (positive when power is injected to the low-inertia area) are modeled similarly to governor/turbine action by

$$\frac{dp^{l\omega}}{dt} = -T_{l\omega}^{-1} (p^{l\omega} - K_{l\omega} u^{cl\omega}) \quad (22)$$

$$u^{cl\omega} = v^{cl\omega} - K_{cl\omega} (N^{\omega} \omega + R_{cl\omega} p^{l\omega}) \quad (23)$$

$$\frac{dv^{cl\omega}}{dt} = -T_{cl\omega}^{-1} K_{cl\omega} (N^{\omega} \omega + R_{cl\omega} p^{l\omega}) \quad (24)$$

where  $N^{\omega}$  is an  $s_1 \times n$  mapping (each row has a single  $+1$  element) that picks up the frequency of the supported area from the vector  $\omega$ . These control dynamics need to be relatively slow to allow the HVDC converters to actuate based on the generated command signals.

In order to transmit the variability of renewable power internally to an interconnection, a number  $s_2$  of HVDC lines is used. These lines are equipped with the following control strategy, which tracks the renewable power with a low-pass filter:

$$\frac{dp^{lr}}{dt} = -T_{lr}^{-1} (p^{lr} - K_{lr} N^r p^r) . \quad (25)$$

For this control strategy to be implementable, it is assumed that the renewable power productions in the areas  $p^r$  (e.g., at the substations of all major wind power plants) can be measured and communicated to the controller. Here, matrices are defined similarly as in the case of the frequency-sensitive HVDC lines. (The powers  $p^{lr}$  are defined positive when power is removed from the low-inertia area.) The injected powers are mapped into areal power injections by

$$p^{dcr} = M^r p^{lr} \quad (26)$$

which is similarly defined as (21).

All derived dynamic expressions, (11), (12)–(14), (20), (22)–(24), (25) are assembled in a system as in (1) with

$$\mathbf{x} = \begin{bmatrix} \omega \\ \theta_\Delta \\ p^g \\ v^{cg} \\ p^{l\omega} \\ v^{cl\omega} \\ p^{lr} \end{bmatrix} \quad (27)$$

and

$$\mathbf{v} = \mathbf{W}\mathbf{w} = \begin{bmatrix} \frac{1}{2}\mathbf{H}^{-1} & -\frac{1}{2}\mathbf{H}^{-1} \\ 0 & 0 \\ 0 & 0 \\ 0 & 0 \\ 0 & 0 \\ 0 & 0 \\ T_{lr}^{-1}\mathbf{N}^r & 0 \end{bmatrix} \begin{bmatrix} p^r \\ w^d \end{bmatrix}. \quad (28)$$

## Case Studies

First, a tractable low-order example is provided. Then the concepts of reachability analysis are applied to the study of a new transmission overlay in the United States. For each case study, reachable sets (zonotopes) and bounds are computed as described in the preceding theoretical section. Deterministic simulations are also run (just for the sake of validation of the proposed technique) with fixed parameters and randomly generated time-varying inputs residing inside given interval sets and/or bounds.

The reported computation times are obtained using an Intel Core i5 CPU running at 3.20 GHz, using MATLAB 2011b [30]. Interval operations were performed using INTLAB [31].

### An Introductory Example

The simplified power system drawn in [26, Fig. 5] is expressed in state-space form as

$$\frac{d\omega}{dt} = -\frac{1}{2h} \left( d + \frac{k_g f_h}{r_c} \right) \omega + \frac{1}{2h} p^g - \frac{1}{2h} w^d \quad (29)$$

$$\frac{dp^g}{dt} = -\frac{k_g(1-f_h)}{r_c \tau_g} \omega - \frac{1}{\tau_g} p^g. \quad (30)$$

Uncertainty is introduced in the damping constant  $d \in \mathbf{d} = [1.8, 2.2]$  p.u., the system inertia  $h \in \mathbf{h} = [3.9, 4.1]$  s, and the load disturbance  $w^d(t) \in \mathbf{w}^d = [0.2, 0.3]$  p.u. The other parameters are treated as fixed values:  $f_h = 0.3$  p.u.,  $k_g = 0.95$  p.u.,  $r_c = 0.05$  p.u.,  $\tau_g = 8$  s.

For this system, the following interval matrix and vectors

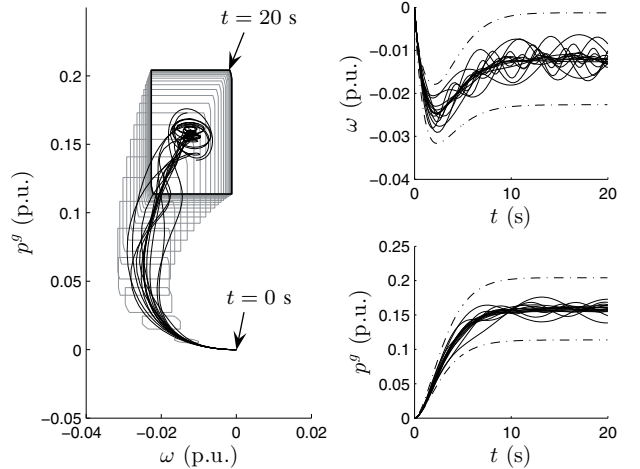


Fig. 4. Zonotopes (gray) and bounds (dashed) for a simple power system.

(rounded to the third decimal digit) are obtained:

$$\begin{aligned} A \in \mathbf{A} &= \begin{bmatrix} [-1.013, -0.914] & [0.122, 0.128] \\ [-1.663-\epsilon_1, -1.663+\epsilon_1] & [-0.125-\epsilon_2, -0.125+\epsilon_2] \end{bmatrix} \\ v \in \mathbf{v} &= \begin{bmatrix} [-0.039, -0.024] \\ [-\epsilon_3, \epsilon_3] \end{bmatrix}, x_0 \in \mathbf{x}_0 = \begin{bmatrix} [-\epsilon_4, \epsilon_4] \\ [-\epsilon_5, \epsilon_5] \end{bmatrix}. \end{aligned} \quad (31)$$

The parameters  $\epsilon_j$  ( $j = 1, \dots, 5$ ) are (small) user-defined positive numbers. The input vector and initial conditions have been written as intervals for compactness of notation, but conversion from an interval vector to a zonotope is necessary.<sup>3</sup> The initial conditions are modeled as small boxes centered at the origin.

Computed zonotopes with a time step  $r = 0.05$  s and time-domain bounds are presented in Fig. 4. Only one out of ten zonotopes has been plotted. All simulated deterministic trajectories (solid lines) remain inside the computed zonotopes and bounds as expected. The total CPU time to simulate 20 s of this 2-state system was approximately 0.5 s.

### Assessments of U.S. Transmission Overlay

A reduced-order model of the continental U.S. power system has been developed, shown in Fig. 5. This model represents the 3 interconnections with 13 regions, and includes existing and new inter-regional transmission capacity. The model parameters, details of interconnection, and line capacities are summarized in Tables I–IV. Parameters were adapted from publicly available information found in [4]–[6], [26], [32]. The existing transmission capacity was approximated based on data found in [5], whereas new HVAC and HVDC overlays were adapted from a national transmission overlay planning study for the year 2020 [33].

Three studies are conducted to illustrate the application of reachability analysis and zonotopes in a bulk power system with the new transmission overlay. First, the frequency-response of area 1 is studied with and without frequency-

<sup>3</sup>To convert an interval vector to a zonotope:  $(c, < g^{(1)}, \dots, g^{(n)} >) = (\text{mid } \mathbf{x}, < \text{diag}(\text{rad } \mathbf{x}) >)$ , where  $\text{mid } \mathbf{x} = 0.5(\underline{\mathbf{x}} + \overline{\mathbf{x}})$  and  $\text{rad } \mathbf{x} = 0.5(\overline{\mathbf{x}} - \underline{\mathbf{x}})$ .



Fig. 5. Reduced national transmission system: existing HVAC (solid), HVAC overlay (dashed), HVDC overlay (dotted).

TABLE I  
PARAMETERS OF EQUIVALENT GENERATORS

Area $i^a$	$h_i^b$	$d_i$	$\tau_{gi}^c$	$k_{gi}$	$r_{ci}$	$\tau_{ci}^c$	$k_{ci}$
1	254.31	3.23	5	75.43	$6.62 \cdot 10^{-4}$	35	1.2
2	532.91	6.66	8	155.30	$3.21 \cdot 10^{-4}$	30	0.9
3	395.87	4.74	7	110.72	$4.51 \cdot 10^{-4}$	32	0.7
4	157.96	2.01	5	46.70	$1.07 \cdot 10^{-3}$	38	0.8
5	112.17	1.29	5	30.10	$1.66 \cdot 10^{-3}$	37	1.4
6	121.21	1.24	6	29.09	$1.71 \cdot 10^{-3}$	37	1.2
7	85.74	0.96	5	22.36	$2.23 \cdot 10^{-3}$	36	1.2
8	158.09	2.03	6	47.35	$1.05 \cdot 10^{-3}$	36	1.5
9	505.82	5.42	8	126.49	$3.95 \cdot 10^{-4}$	30	0.8
10	302.73	3.69	7	86.21	$5.79 \cdot 10^{-4}$	35	0.6
11	314.34	2.14	5	50.02	$9.99 \cdot 10^{-4}$	30	0.7
12	155.84	1.77	6	41.27	$1.21 \cdot 10^{-3}$	30	1.3
13	216.66	2.08	4	48.48	$1.03 \cdot 10^{-3}$	30	1.4

<sup>a</sup> Values are in p.u. on a 1000-MVA base.

<sup>b</sup> Inertia constants in s.

<sup>c</sup> Time constants in s.

TABLE II  
EXISTING HVAC TRANSMISSION

Line $(i - j)$	Cap. <sup>a</sup>	$b_{ij}^b$	Line $(i - j)$	Cap. <sup>a</sup>	$b_{ij}^b$
2 – 3	9.50	14.78	5 – 10	1.49	1.32
2 – 4	12.7	19.63	6 – 7	1.89	2.93
2 – 9	8.60	13.35	8 – 9	3.6	5.60
3 – 6	3.44	5.34	9 – 10	5.61	8.73
3 – 9	2.60	4.04	11 – 12	1.34	2.08
4 – 5	1.73	2.69	11 – 13	9.18	14.28
4 – 9	4.62	7.18	12 – 13	8.32	12.93
4 – 10	1.20	1.87			

<sup>a</sup> Transmission capacity in p.u. on a 1000-MVA base.

<sup>b</sup> Equivalent line susceptance in p.u.

sensitive HVDC lines. The HVAC overlay (Table III) is not included in this study. In the second study, we focus on the dynamic response of the Eastern interconnection with new HVAC and embedded HVDC lines transmitting the variability of wind sources. Finally, a study is performed at steady state, which illustrates bounds of power flows in transmission lines under uncertain renewable power injections. The results are in p.u. on a 1000-MVA base.

**Study 1: Frequency-sensitive HVDC.** The disturbance in area 1 is an unknown-but-bounded renewable power drop (step change at  $t = 0$ ) inside the arbitrarily selected range

TABLE III  
HVAC TRANSMISSION OVERLAY

Line $(i - j)$	Cap. <sup>a</sup>	$b_{ij}^b$	Line $(i - j)$	Cap. <sup>a</sup>	$b_{ij}^b$
2 – 3	4.20	6.53	4 – 10	1.80	2.80
2 – 4	1.83	2.84	5 – 9	1.20	1.86
2 – 5	3.00	4.52	5 – 10	2.40	3.73
2 – 6	1.20	1.86	6 – 7	2.50	3.88
2 – 9	4.20	6.53	6 – 9	0.60	0.93
2 – 10	2.70	4.20	8 – 9	0.60	0.93
3 – 6	4.00	6.22	8 – 10	0.60	0.93
3 – 9	1.00	1.55	11 – 12	0.60	0.93
4 – 5	1.50	2.33	11 – 13	0.60	0.93
4 – 9	1.20	1.86	12 – 13	1.20	1.86

<sup>a</sup> Transmission capacity in p.u. on a 1000-MVA base.

<sup>b</sup> Equivalent line susceptance in p.u.

TABLE IV  
HVDC TRANSMISSION OVERLAY

Line $(i - j)$	Type	$r_{cl\omega}$	$k_{l\omega/r}$	$\tau_{l\omega/r}$	$k_{cl\omega}$	$\tau_{cl\omega/r}$
1 – 10	freq.	0.025	2	0.9	3	5
1 – 12	freq.	0.025	2	0.9	3	5
2 – 5	var.	N/A	1	0.3	N/A	N/A

$p_1^r(t) \in p_1^r = [-750, -650]$  MW [4]. The variability-sensitive line, 2 – 5, is disabled for this study. Figures 6 and 7 contrast the response of area-1 frequency  $\omega_1$  without and with dynamic support through the HVDC lines that connect this area to two neighboring areas (10 and 12 in Fig. 5).

It can be observed that there is improvement in the minimum frequency of area 1, suggesting that the high-capacity HVDC links with frequency regulation capability are beneficial in this aspect. In the former case, the lower frequency bound can drop by almost 0.01 p.u. (59.4 Hz), which is a common threshold for under-frequency relaying tripping. In the latter case, the minimum frequency is higher, thus providing a larger safety margin. Figure 8 shows projections of the reachable sets of the frequencies of three arbitrarily selected areas (in case a frequency-sensitive HVDC overlay is in place), to illustrate the propagation of an area-1 disturbance to the other interconnections. Figure 9 shows time-domain bounds of the HVDC dynamic power injections into area 1, which are on the order of 100 MW each, a substantially lower value than the disturbance itself. It should be noted that these results were obtained with only a basic control tuning process, and it might be possible to further improve the frequency response with more advanced control techniques.

The same study is repeated by adding a  $\pm 5\%$  uncertainty in the inertia constant of area 1. Figure 10 should be compared with Fig. 7. The reachable sets have grown due to the pessimism introduced by the uncertainty regarding the inertia.

For these studies a time step  $r = 0.01$  s was used and only one out of one hundred zonotopes has been plotted. The CPU time to simulate 100 s of this 53-state system was 14 min.

**Study 2: HVAC and variability-sensitive HVDC.** In this case study, we apply an unknown-but-bounded step disturbance that represents a loss of renewable generation in the arbitrarily

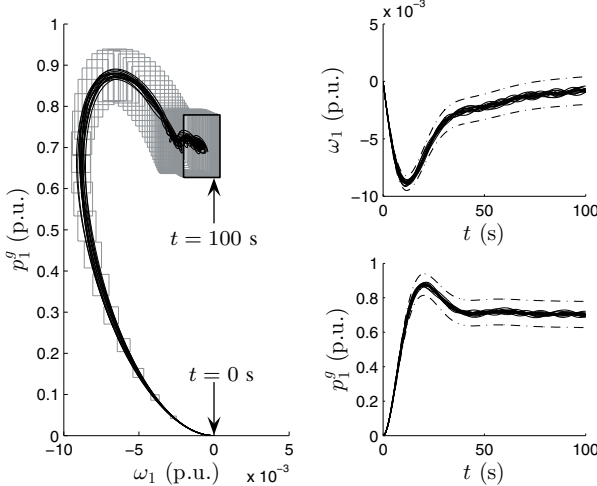


Fig. 6. Area-1 response without frequency-sensitive HVDC interconnection (i.e., the HVDC lines just inject a fixed amount of power): zonotopes (gray), time-domain bounds (dashed), and deterministic trajectories (solid).

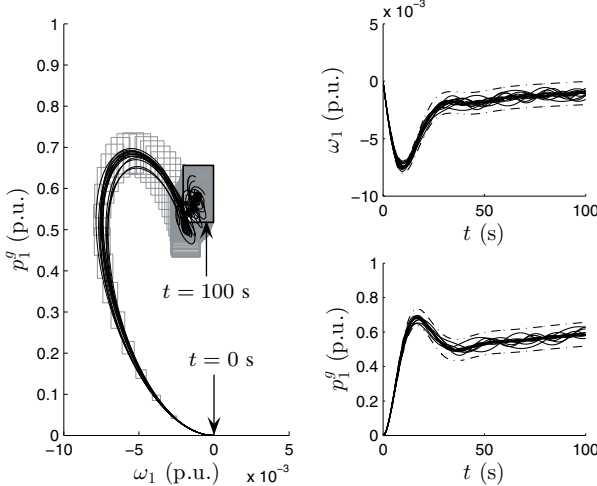


Fig. 7. Area-1 response with frequency-sensitive HVDC interconnection: zonotopes (gray), time-domain bounds (dashed), and deterministic trajectories (solid).

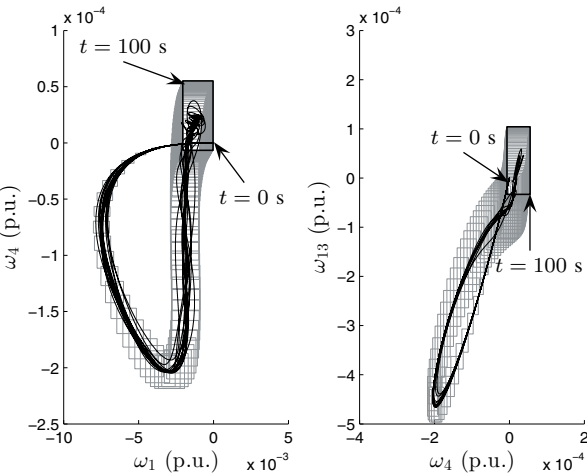


Fig. 8. Evolution of selected zonotope projections (gray) and deterministic trajectories (solid) with HVDC-overlay frequency support to area 1.

selected range  $p_5^r(t) \in \mathbf{p}_5^r = [-600, -300]$  MW in area 5. To obtain a step-like behavior,  $p_5^r$  is modeled as an extra state

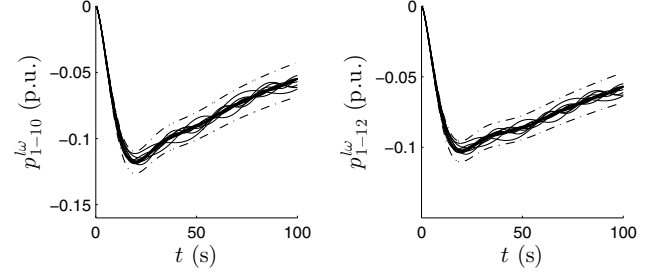


Fig. 9. Response of frequency-sensitive HVDC lines supporting area 1: time-domain bounds (dashed) and example trajectories (solid).

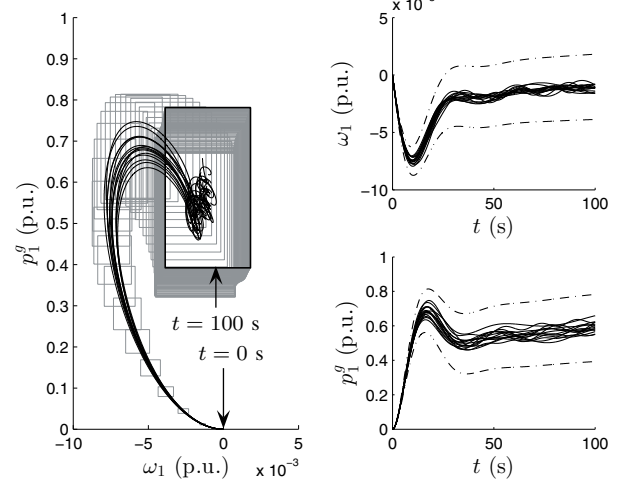


Fig. 10. Area-1 response with frequency-sensitive HVDC interconnection and inertia constant uncertainty ( $\pm 5\%$ ): zonotopes (gray), time-domain bounds (dashed), and deterministic trajectories (solid).

with  $\frac{d}{dt}p_5^r = 0$  and initial condition bounds equal to  $\mathbf{p}_5^r$ . Figure 11 shows time-domain bounds of the response of area 5 when HVAC/HVDC overlays are not in service. It is interesting to note that the bounds themselves exhibit an oscillatory behavior. Figure 12 shows similar plots when the HVAC overlay only is in place. It can be observed that the addition of HVAC lines has changed the oscillatory behavior of the system (as expected). Figure 13 shows dynamic results of area 5 when the HVDC line 2 – 5 is in service but without HVAC overlay. In this case, the HVDC line improves the damping of the response slightly; better damping performance could be achieved with more advanced control design, such as a wide-area controller, but such analysis is outside the scope of the present study. Figure 14 shows the dynamic response of the HVDC line.

To generate these results, a time step  $r = 0.01$  s was used. The CPU time to simulate 20 s of a 51-state system was approximately 1.3 min.

*Study 3: Steady-state analysis.* In this study, steady-state conditions are considered.<sup>4</sup> The HVDC overlay is not in place.

<sup>4</sup>This is not a study of power system dynamics per se, but is included in the paper to demonstrate an interesting application of zonotopes.

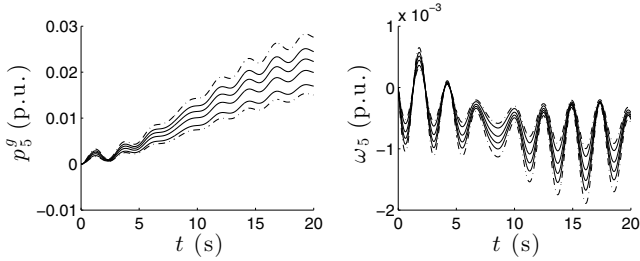


Fig. 11. Area-5 response without HVAC/HVDC overlay: time-domain bounds (dashed) and example trajectories (solid).

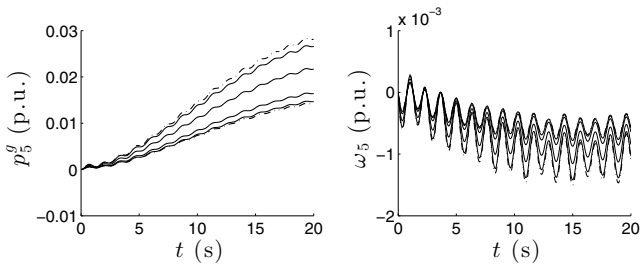


Fig. 12. Area-5 response with HVAC overlay: time-domain bounds (dashed) and example trajectories (solid).

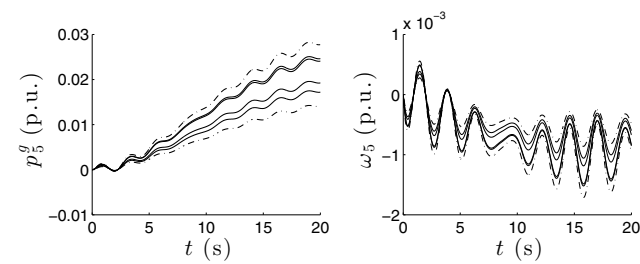


Fig. 13. Area-5 with HVDC line 2 – 5: time-domain bounds (dashed) and example trajectories (solid).

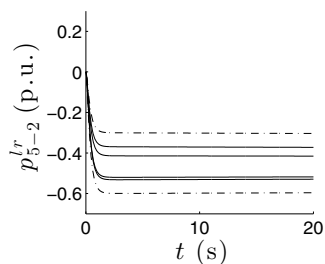


Fig. 14. HVDC line 5 – 2 dynamic response: time-domain bounds (dashed) and example trajectories (solid).

At steady state,

$$x_{ss} = -A^{-1}v_{ss}, \quad (32)$$

where \$v\_{ss}\$ represents an unknown-but-bounded *constant* input and \$A\$ is assumed to be known precisely. Given unknown power injections \$p^r\$, a zonotope that includes all possible states can be calculated using (28) and (32). We extract the zonotope of \$\theta\_\Delta\$ from the zonotope of \$x\$, then using information of the system topology we obtain zonotopes of power flows in

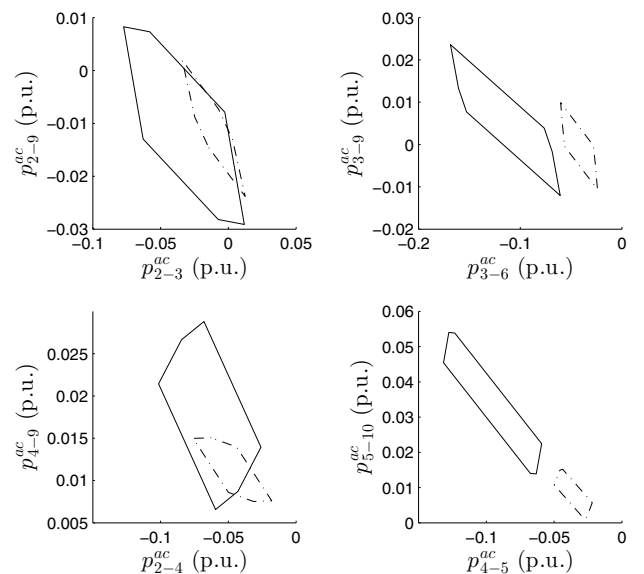


Fig. 15. Example of possible steady-state power flows in existing HVAC transmission lines without (solid) and with (dashed) HVAC overlay by uncertain renewable power injections.

individual HVAC lines. It should be noted that this calculation is exact, since no over-approximations are involved in the calculations.

In this example, the unknown-but-bounded power injections are \$p\_5^r, p\_7^r, p\_{10}^r \in [100, 200]\$ MW (independent of each other). Two-dimensional projections of the zonotopes enclosing the power flows of select transmission lines are plotted in Fig. 15 for cases with and without HVAC overlay, respectively. When an HVAC overlay is added, the zonotopes shrink because power is shared between the existing and new lines.

## Conclusion

This work presented a computational method using reachability analysis theory with zonotopes for conducting assessments of the impact of new high-capacity transmission on power system frequency dynamics. The method allows the analyst to incorporate a wide range of uncertainties (parametric and operational) that are inherently present in the planning stage. Extensions of the technique for the analysis of larger-scale and/or nonlinear systems are possible and worthwhile to investigate further.

## Acknowledgments

The work described in this paper was made possible by funding provided by the U.S. Department of Energy for “The Future Grid to Enable Sustainable Energy Systems,” an initiative of the Power Systems Engineering Research Center. Also, support for this research was provided by a National Science Foundation Research Experience for Undergraduates site program in “Wind Energy Science Engineering and Policy (WESEP)” grant number EEC-1063048 at Iowa State University.

## Appendix

- 1) Zonotopes are closed under linear transformations. If  $M$  is a linear map, the linear transformation of a zonotope  $\mathcal{Z}$  is [21]:

$$\begin{aligned} M\mathcal{Z} &= \left\{ Mx : x = c + \sum_{i=1}^p \alpha_i g^{(i)}, -1 \leq \alpha_i \leq 1 \right\} \\ &= \left( Mc, \langle Mg^{(1)}, \dots, Mg^{(p)} \rangle \right). \end{aligned} \quad (33)$$

If an interval matrix  $M$  is expressed in the form  $M = \check{M} + [-\hat{M}, \hat{M}]$ , i.e., a center plus a symmetric interval matrix, then an over-approximation of the mapping of a zonotope through the interval linear transformation represented by  $M$  is [22]:

$$M\mathcal{Z} = \left( \check{M}c, \langle \check{M}g^{(1)}, \dots, \check{M}g^{(p)}, w^{(1)}, \dots, w^{(n)} \rangle \right) \quad (34)$$

where

$$w_j^{(i)} = \begin{cases} 0 & \text{if } i \neq j \\ (\hat{M}_{j:}) \cdot (|c| + \sum_{k=1}^p |g^{(k)}|) & \text{if } i = j \end{cases} \quad (35)$$

The notation  $w_j^{(i)}$  stands for the  $j^{\text{th}}$  element of the vector  $w^{(i)}$ , and  $\hat{M}_{j:}$  denotes the  $j^{\text{th}}$  row of  $\hat{M}$ .

- 2) Zonotopes are closed under the Minkowski sum. If  $\mathcal{Z}_1 = (c^{(1)}, \langle g^{(1)}, \dots, g^{(p)} \rangle)$  and  $\mathcal{Z}_2 = (c^{(2)}, \langle h^{(1)}, \dots, h^{(q)} \rangle)$ , then [21]:

$$\begin{aligned} \mathcal{Z}_1 \oplus \mathcal{Z}_2 &= \left( c^{(1)} + c^{(2)}, \langle g^{(1)}, \dots, g^{(p)}, \right. \\ &\quad \left. h^{(1)}, \dots, h^{(q)} \rangle \right). \end{aligned} \quad (36)$$

Appropriate reduction techniques should be employed to control the zonotope generators' expansion when this operation is employed iteratively [21].

## References

- [1] J. McCalley, J. Bushnell, V. Krishnan, and S. Cano, "Transmission design at the national level: Benefits, risks, and possible paths forward," White Paper, PSERC, Jan. 2012.
- [2] V. Krishnan, J. McCalley, S. Lemos, and J. Bushnell, "Nation-wide transmission overlay design and benefits assessment for the U.S." *Energy Policy*, vol. 56, pp. 221–232, May 2013.
- [3] B. Parsons *et al.*, "Grid impacts of wind power variability: Recent assessments from a variety of utilities in the United States," National Renewable Energy Laboratory, Tech. Rep. NREL/CP-500-39955, Jul. 2006.
- [4] J. M. Undrill *et al.*, "Power and frequency control as it relates to wind-powered generation," Lawrence Berkeley National Laboratory, Tech. Rep. LBNL-4143E, Dec. 2010.
- [5] P. Mackin *et al.*, "Dynamic simulation studies of the frequency response of the three U.S. interconnections with increased wind generation," Lawrence Berkeley National Laboratory, Tech. Rep. LBNL-4146E, Dec. 2010.
- [6] J. H. Eto *et al.*, "Use of frequency response metrics to assess the planning and operating requirements for reliable integration of variable renewable generation," Lawrence Berkeley National Laboratory, Tech. Rep. LBNL-4142E, Dec. 2010.
- [7] T. Machida, Y. Yoshida, and H. Nakamura, "A method of automatic frequency ratio control by a DC system," *IEEE Trans. Power App. Syst.*, vol. PAS-86, no. 3, pp. 263–267, Mar. 1967.
- [8] M. Sanpei, A. Kakehi, and H. Takeda, "Application of multi-variable control for automatic frequency controller of HVDC transmission system," *IEEE Trans. Power Del.*, vol. 9, no. 2, pp. 1063–1068, Apr. 1994.
- [9] K. Y. Lim, Y. Wang, and R. Zhou, "Decentralised robust load-frequency control in coordination with frequency-controllable HVDC links," *Int. J. Elect. Power and Energy Syst.*, vol. 19, no. 7, pp. 423–431, 1997.
- [10] L. Fan, Z. Miao, and D. Osborn, "Wind farms with HVDC delivery in load frequency control," *IEEE Trans. Power Syst.*, vol. 24, no. 4, pp. 1894–1895, Nov. 2009.
- [11] J. Dai, Y. Phulpin, A. Sarlette, and D. Ernst, "Impact of delays on a consensus-based primary frequency control scheme for AC systems connected by a multi-terminal HVDC grid," in *Proc. IREP Symp. Bulk Power Syst. Dynamics and Control - VIII*, Buzios, RJ, Brazil, Aug. 2010.
- [12] P. Varaiya, "Reach set computation using optimal control," in *KIT Workshop Verification Hybrid Syst.*, Grenoble, France, Oct. 1998.
- [13] A. Chutinan and B. H. Krogh, "Computing polyhedral approximations to flow pipes for dynamic systems," in *Proc. 37th IEEE Conf. Decision and Control*, vol. 2, Dec. 1998, pp. 2089–2094.
- [14] Z. Han and B. H. Krogh, "Reachability analysis of nonlinear systems using trajectory piecewise linearized models," in *Proc. 2006 American Control Conf.*, Minneapolis, Jun. 2006.
- [15] P. M. Anderson and A. Bose, "A probabilistic approach to power system stability analysis," *IEEE Trans. Power App. Syst.*, vol. PAS-102, no. 8, pp. 2430–2439, Aug. 1983.
- [16] R. Billinton, M. Fotuhi-Firuzabadi, and L. Bertling, "Bibliography on the application of probability methods in power system reliability evaluation 1996–1999," *IEEE Trans. Power Syst.*, vol. 16, no. 4, pp. 595–602, Nov. 2001.
- [17] J. Hockenberry and B. Lesieutre, "Evaluation of uncertainty in dynamic simulations of power system models: The probabilistic collocation method," *IEEE Trans. Power Syst.*, vol. 19, no. 3, pp. 1483–1491, Aug. 2004.
- [18] A. Kurzhanski and P. Varaiya, "On ellipsoidal techniques for reachability analysis," *Optimization Methods and Software*, vol. 17, pp. 177–237, 2000.
- [19] ———, "Ellipsoidal techniques for reachability analysis of discrete-time linear systems," *IEEE Trans. Autom. Control*, vol. 52, no. 1, pp. 26–38, Jan. 2007.
- [20] Y. C. Chen and A. D. Domínguez-García, "A method to study the effect of renewable resource variability on power system dynamics," *IEEE Trans. Power Syst.*, vol. 27, pp. 1978–1989, Nov. 2012.
- [21] A. Girard, "Reachability of uncertain linear systems using zonotopes," in *Proc. 8th Int. Conf. on Hybrid Systems*, Zurich, Switzerland, 2005, pp. 291–305.
- [22] M. Althoff, O. Stursberg, and M. Buss, "Reachability analysis of linear systems with uncertain parameters and inputs," in *Proc. 46th IEEE Conf. on Decision and Control*, New Orleans, Dec. 2007, pp. 726–732.
- [23] R. B. Kearfott *et al.* (2010) Standardized notation in interval analysis. [Online]. Available: [http://interval.louisiana.edu/preprints/Shary\\_n.pdf](http://interval.louisiana.edu/preprints/Shary_n.pdf)
- [24] C. L. Guernic, "Reachability analysis of hybrid systems with linear continuous dynamics," Ph.D. dissertation, Université Grenoble 1 - Joseph Fourier, Oct. 2009.
- [25] M. Althoff, "Reachability analysis and its application to the safety assessment of autonomous cars," Ph.D. dissertation, Technischen Universität München, Feb. 2010.
- [26] P. Anderson and M. Mirheydar, "A low-order system frequency response model," *IEEE Trans. Power Syst.*, vol. 5, pp. 720–729, Aug. 1990.
- [27] A. J. Wood and B. F. Wollenberg, *Power Generation, Operation, and Control*, 2nd ed. New York: John Wiley & Sons, 1996.
- [28] H. Bevrani, *Robust Power System Frequency Control*. New York: Springer, 2009.
- [29] IEEE Committee Report, "Dynamic models for steam and hydro turbines in power system studies," *IEEE Trans. Power App. Syst.*, vol. PAS-92, no. 6, pp. 1904–1915, Nov. 1973.
- [30] (2011) MATLAB R2011b. The MathWorks Inc. Natick, MA. [Online]. Available: [www.mathworks.com](http://www.mathworks.com)
- [31] S. M. Rump, "INTLAB - INTerval LABoratory," in *Developments in Reliable Computing*, T. Csendes, Ed. Dordrecht: Kluwer Academic Publishers, 1999, pp. 77–104.
- [32] Generation by state. Energy Information Administration (EIA). [Online]. Available: <http://www.eia.gov/electricity/data.cfm#gencapacity>
- [33] Y. Li, "A national transmission overlay," Jun. 2012, private communication at Iowa State University.